Supplementary Material

1 TRANSFORMATION BETWEEN FRAMES

In Section 2, we have defined three coordinate systems, earth-fixed frame, vehicle-body frame, and the sensor frame. The earth fixed reference frame ($X_e - Y_e - Z_e$) is selected in a North-East-Down (NED) convention with its x-axis pointing towards geographic North, y-axis pointing East, and z-axis pointing downward. The origin of this reference frame is free to choose but fixed to the local water surface (zero depth) at known latitude and longitude. The vehicle frame ($X_v - Y_v - Z_v$) is located at the center of gravity of the USV SEADRAGON with the x-axis pointing forward, y-axis pointing starboard, and z-axis pointing downward. For each sensor, we define a sensor frame ($X_s - Y_s - Z_s$) having the same orientation as the vehicle frame, but offset by a translation vector ${}^{v}_{s}\mathbf{T}$ from the origin of the vehicle frame.

A detailed sketch showing the transformation between frames is presented in Figure S1. For a range vector, $\mathbf{r}_t$, as reported by the sonar or the LIDAR at time t, we convert it into a point vector, ${}^{v}\mathbf{P}_t$, in the vehicle frame using Equation S1 with σ_t being the angle between the range vector and $X_s - Y_s$ plane and β_t being the angle between the range vector and $Y_s - Z_s$ plane. The point vector, ${}^{v}\mathbf{P}_t$, could be further converted into the earth frame using Equation S2 where ϕ_t, θ_t, and ψ_t are the vehicle roll, pitch, and yaw, and ${}^{e}_{v}\mathbf{T}$ is the displacement of the origin of the vehicle frame relative to the chosen origin of the earth fixed reference frame.

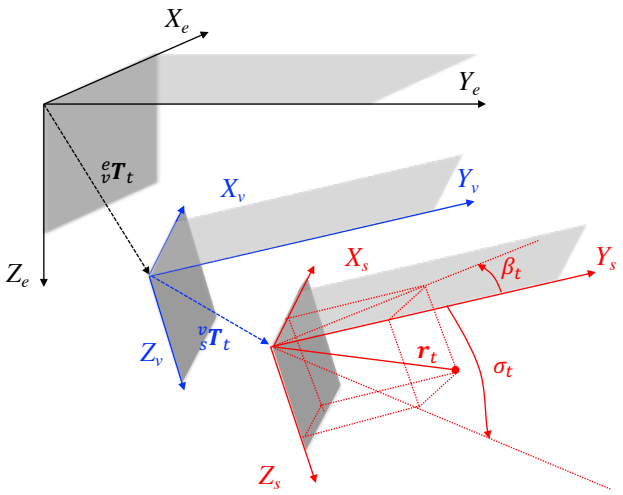

Figure S1. Conversion between the Earth frame ($X_e - Y_e - Z_e$), the vehicle frame ($X_v - Y_v - Z_v$), and the sensor frame ($X_s - Y_s - Z_s$).

$$ {}^{v}\mathbf{P}_t = \mathbf{R}_z(\beta_t)\,\mathbf{R}_x(\sigma_t)\mathbf{r}_t + {}^{v}_{s}\mathbf{T} \tag{S1} $$

$$ {}^{e}\mathbf{P}_t = \mathbf{R}_x(\phi_t)\,\mathbf{R}_y(\theta_t)\,\mathbf{R}_z(\psi_t)\,{}^{v}\mathbf{P}_t + {}^{e}_{v}\mathbf{T}_t \tag{S2} $$

2 SENSOR SETUP AND DATA INFORMATION

During operations, the USV SEADRAGON navigates using a Global Positioning System (GPS) on the top deck, and the orientation is estimated using an Attitude Heading Reference System (AHRS) calibrated to the origin of the vehicle frame, the center of gravity of the vehicle. The sonar and LIDAR both produce range measurements from the vehicle to the iceberg surface. As shown in Figure S2, the sonar is mounted on the lower hull with a vertical field-of-view on the starboard side of the vehicle. Its view angle covers from horizontal (0 deg) to 130 degrees downwards with a resolution of 1.8 degrees. The sonar data is processed in real-time with a sonar ping rate of 0.5 Hz at a profiling range of 150 meters. The LIDAR is located on the top deck with the maximum profiling range of 100 meters. It has a vertical field-of-view of 30 degrees with 2 degrees angular resolution, and it performs horizontal scanning of 360 degrees at 600 RPM with a stepping angle of 0.4 degrees. In Table S1, we have summarized the parameters for the profiling sensors. Using these values, we could convert all the measurements produced by the sonar and LIDAR into the earth-fixed frame.

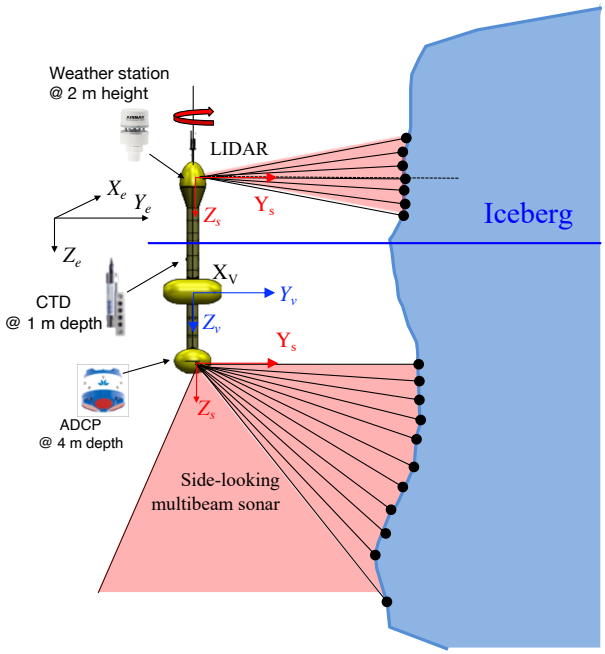

Figure S2. Sensor locations on the SEADRAGON.

Table S1. Sonar and LIDAR configuration summary

	Multibeam sonar	LIDAR
Sampling speed	0.5 Hz	600 RPM
σ range	0 to 130 deg	-15 to 15 deg
σ step	0.18 deg	2 deg
β range	0 deg	0 to 360 deg
β step	0	0.4 deg
Profiling range	150 m	100m
Mounting offset	$[0.71, 0.18, 2.06]^T$ m	$[0.28, 0, -3.6]^T$ m

The data summary for the mapping sensors is presented in Table S2. The sonar was configured with a profiling range of 150 m with a ping interval of about 2 seconds. In contrast, the LIDAR was scanning at 10 Hz with a profiling range of about 100 m. Due to the sampling rate difference, the LIDAR data points is 20 times more than the sonar points. Because the sonar has a wide vertical field-of-view, the seafloor is also mapped. We have shown the sonar data points in Figure S3. The seafloor point clouds could be easily identified below 60 meters. These data points are excluded from our motion estimation algorithm. The number of used data points is around 40% percent of the total number.

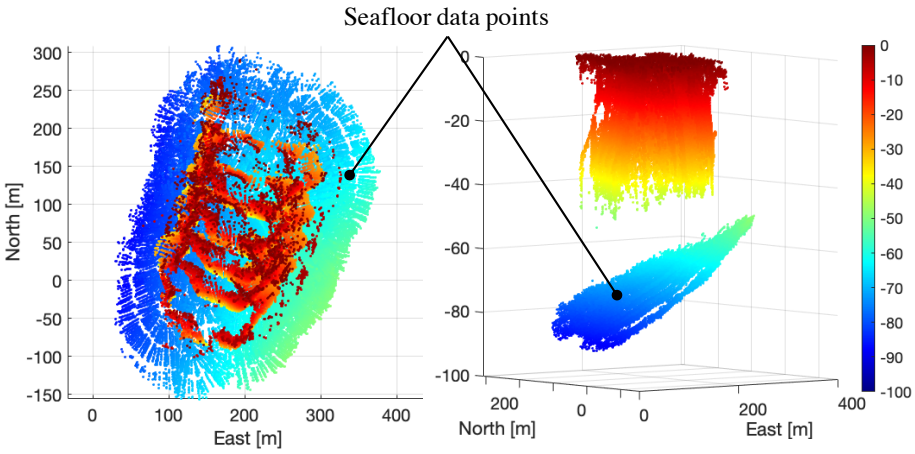

Figure S3. Seafloor data points collected by the sonar

Table S2. Sonar and LIDAR configuration during the mission

	Sonar	LIDAR
Manufacturer	Teledyne Blueview	Velodyne
Configured profiling range	150 m	100 m
Sampling speed	0.5Hz	10Hz
Sensor on time	15:23:19	15:31:24
Senor off time	16:49:01	16:57:17
Total data points	681,096	23,724,944
Used data points	278,621	23,724,944

In Table S3, we summarize the scientific instrument and the measurements. The weather station, located on the top deck, measures the atmospheric information, including the air temperature and wind speed. The CTD is submerged at 1 meter measuring surface water properties. The ADCP was mounted in the bottom hull. The ADCP frequency is operated at 600 kHz at a profiling range of 50 meters with a 2 meters depth bin. These sensors were sampled at different intervals. Data processing was discussed in detail in Section 5.

Figure S4 presents the comparison between the images taken around the iceberg and the rendered iceberg shape. The arrows highlight the common features found in the photos and our iceberg rendering. In contrast, the red rectangles show missing features from our iceberg render. The uncovered iceberg tip may exceed the field-of-view (30 degrees) of the LIDAR.

Table S3. Science sensors specification and data summary

	Weather station	CTD	ADCP
Manufacturer	AirMar	SeaBird	RDI 600 kHz
Profiling range	in-situ	in-situ	0 to 50 m
Sampling speed	2Hz	4Hz	18 seconds
Mounting offset	$[0, 0, 2]^T$	$[0, 0, 1]^T$	$[0, 0, 4]^T$
Sensor on time	15:27:43	15:27:42	15:27:54
Sensor off time	16:49:00	16:49:00	16:48:54
Data points	9,392	19,512	5,420

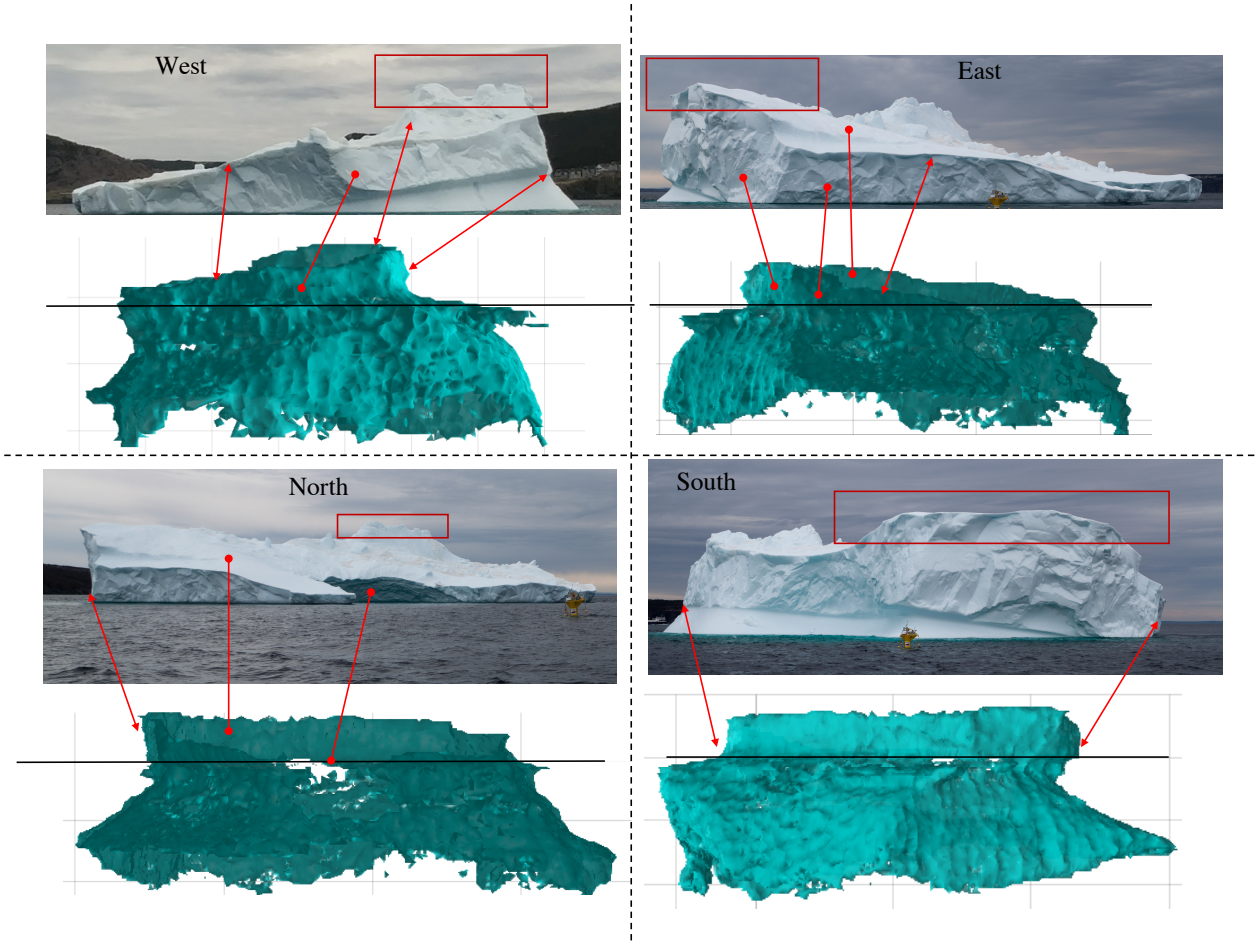

Figure S4. Comparison between the images and the rendered iceberg shape

3 ICEBERG MELT COMPUTATION

In this section, we present the detailed information on the iceberg melt rate computation as described in Section 5 of the paper. We present all the math symbols and their values in Table S4.

As described in Stern et al. (2015), relation between the melt rate, $\dot{m}$ and the energy, B, can be expressed in Equation S3.

$$B = \dot{m}\, L\, \rho_i \tag{S3}$$

Table S4. Definition and values for the constants related to melt rate computation

Symbol	Definition	value	Source
ρ_a	air density $[kg/m^3]$	1.253	Stern et al. (2015)
c_{pa}	specific heat of air $[\frac{J}{kgK}]$	1006.1	Stern et al. (2015)
A	Dimensionless transfer coefficient for air[non-dim]	0.003	Stern et al. (2015)
$V_a(\theta)$	air flow speed [m/s]	Figure S5(A)	in-situ weather station
T_a	Air temperature (averaged) [^{o}C]	8.15	in-situ weather station
T_{fa}	Air freezing point[^{o}C]	0	assumed constant
$\rho_w(\theta)$	water density $[kg/m^3]$	Figure S5(C)	in-situ CTD
c_w	specific heat of air $[\frac{J}{kgK}]$	3970	Stern et al. (2015)
St_*	Stanton number [non-dim]	0.0057	McPhee (2008)
C_d	iceberg drag coefficient[non-dim]	0.0015	Holland and Jenkins (1999)
$V_b(\theta)$	current velocity [m/s]	Figure S5(B)	in-situ ADCP
$T_b(\theta)$	water temperature [^{o}C]	Figure S5(D)	in-situ CTD
$T_f(\theta)$	water freezing temperature [^{o}C]	-1.7	averaged value
L	Latent heat of ice [J/kg]	333,500	McPhee (2008)
ρ_i	ice density $[kg/m^3]$	920	Barker et al. (2004)

For the above-water part, the energy consists of four components induced by shortwave radiation, long-wave radiation, sensible heat flux and latent heat flux. In our study, we only consider the sensible heat flux induced melting here. The latent heat flux is much smaller than the shortwave radiation and sensible heat flux (Van de Wal and Russell, 1994). The shortwave and long-wave radiation induced terms are related to the Albedo parameter. The sensible heat flux for the above water portion can be expressed in Equation S4 [Paterson,1994] with respect to the sections at different azimuth anglee, θ. The constants, ρ_a, c_{pa}, T_{fa}, and A are defined in Table S4. Slightly temperature difference (less than 0.5 degrees) was observed from the weather station. Therefore, we use a constant air temperature T_a of 8.15^oC, averaged from the measurements. The air-speed, $u_a(\theta)$, is obtained from the weather station measurements.

$$H_a(\theta) = \rho_a \, c_{pa} \, A \, V_a(\theta)(T_a - T_{fa}) \tag{S4}$$

For the below water part, the sensible heat could is computed using Equation S5 where the water density, $\rho_w(\theta)$ is obtained from the CTD data, u_w is the overall flow speed computed from the ADCP data, T_w is the water temperature obtained from the CTD data, and the T_f is the freezing point of the water computed based on the salinity and pressure measured by the CTD.

$$H_b = \rho_w(\theta) c_w (St_* \sqrt{C_d}) V_b(\theta)(T_w(\theta) - T_f(S_w(\theta), P(\theta)) \tag{S5}$$

Using Equation S3, we could compute the above and below water melt rates, $\dot{m}_a$ and $\dot{m}_b$, due to the sensible heat flux, H_a and H_b.

Beyond the sensible heat flux, we also computed the melt rate due to surface wave erosion, as shown in Equation S6 (Savage, 2001; Scambos et al., 2008) where it is estimated to be 1 m/day per degree above the freezing temperature.

$$\dot{m}_s = T_b(\theta) - T_f(\theta) \tag{S6}$$

In Equation S7, we compute the total melt volume based on the melt rates and their associated iceberg surface area. Herein, we assume the iceberg is represented in stacked layers. Using the final gridded data points shown in Section 5, we could compute the contour line length in each section at incremental depth. Then, the sectional surface area is computed by integrating the multiplication of the section contour length and the depth interval. In our computation, we select the section width to be 10 degrees and the depth interval to be 1 meter. For the above-water melt volume, the associated surface area is the above portion. For the below-water melt volume, the associated surface area is up to 50 meters. For the surface erosion melt volume, the associated surface area is from the mean height above the water to 15 meters depth (assumed thermocline lower bound). The total melt volume is estimated to be $1.088 \times 10^5 m^3/day$.

$$\dot{V} = \sum_{\theta=0^o}^{360^o} \frac{\rho_i}{\rho_w(\theta)} (\dot{m}_s(\theta) A_s(\theta) + \dot{m}_a(\theta) A_a(\theta) + \dot{m}_b(\theta) A_b(\theta)) \tag{S7}$$

Figure S5 presents all the melting metrics as a function of the azimuth angle. Meanwhile, we could compute the total iceberg volume by integrating the contour area over the depth interval. The total melt volume could be estimated by adding the sectional melt volumes. The estimated iceberg volume is $5.87 \times 10^5 m^3$.

REFERENCES

Barker, A., Sayed, M., and Carrieres, T. (2004). Determination of iceberg draft, mass and cross-sectional areas. In *The Fourteenth International Offshore and Polar Engineering Conference*. 899–904

Holland, D. M. and Jenkins, A. (1999). Modeling thermodynamic ice-ocean interactions at the base of an ice shelf. *Journal of Physical Oceanography* 29, 1787–1800

McPhee, M. G. (2008). *Air-Ice-Ocean Interaction: Turbulent Ocean Boundary Layer Exchange Processes* (ISBN 978-0-387-78334-5, Springer)

Savage, S. B. (2001). Aspects of iceberg deterioration and drift. *Geomorphological Fluid Mechanics, Lecture Notes* 582, 279–318

Scambos, T., Ross, R., Bauer, R., Yermolin, Y., Skvarca, P., Long, D., et al. (2008). Calving and ice-shelf break-up processes investigated by proxy:antarctic tabular iceberg evolution during northward drift. *Journal of Glaciology* 54, 579–591

Stern, A., Johnson, E., Holland, D. M., Wagner, T. J., Wadhams, P., Bates, R., et al. (2015). Wind-driven upwelling around grounded tabular icebergs. *Journal of Geophysical Research: Oceans* 120, 5820–5835

Van de Wal, R. S. W. and Russell, A. J. (1994). A comparison of energy balance calcula- tions, measured ablation and meltwater runoff near sndre strmfjord, west greenland. *Global and planetary change* 9, 29–38

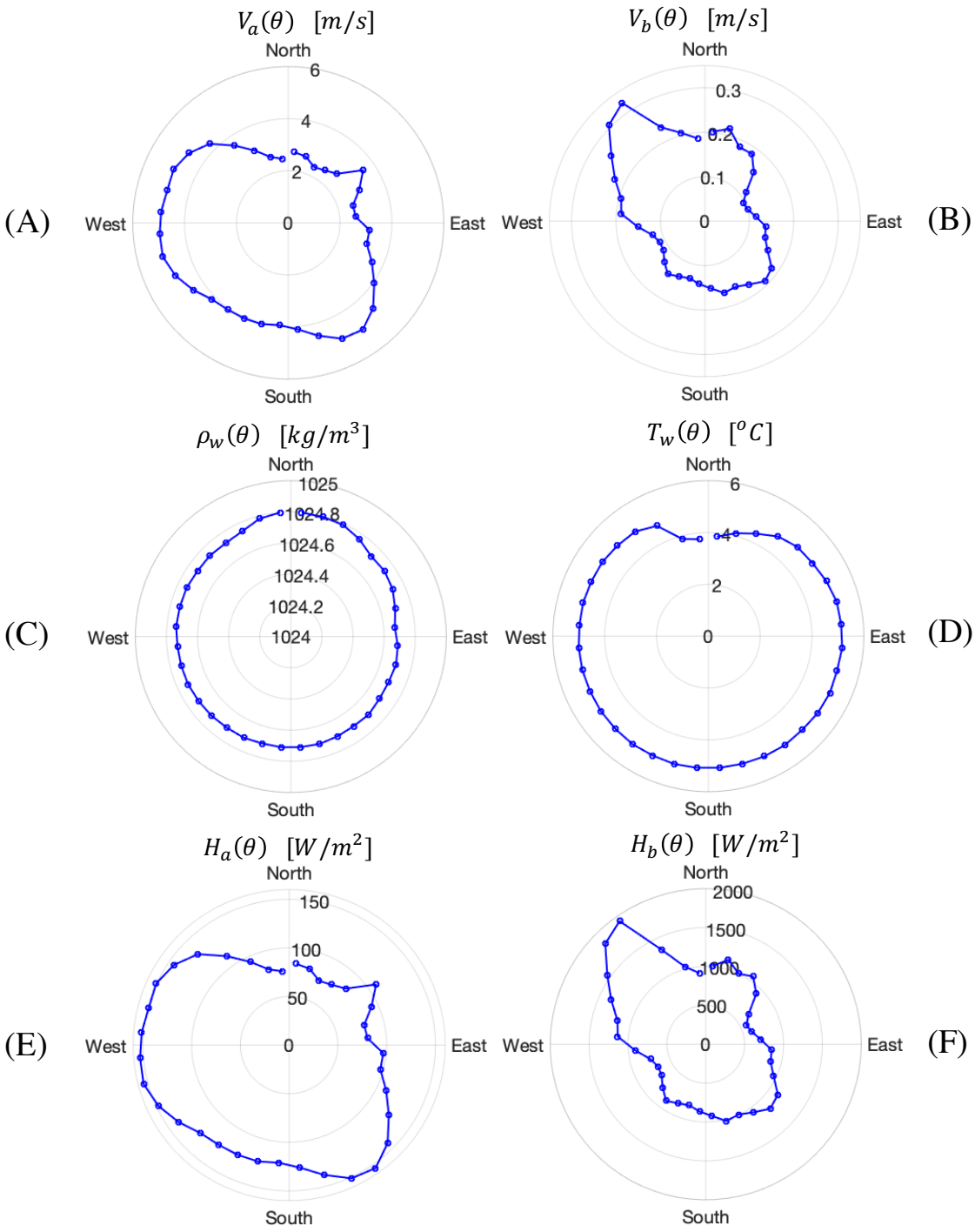

Figure S5. Azimuth angle related parameters for the melt rate computation.